Journal of Power Sources 232 (2013) 132–138

Contents lists available at SciVerse ScienceDirect

Journal of Power Sources

journal homepage: www.elsevier.com/locate/jpowsour

Enhanced performance of activated carbon–polytetrafluoroethylene air-cathode by avoidance of sintering on catalyst layer in microbial fuel cells

Heng Dong, Han Yu, Hongbing Yu**, Ningshengjie Gao, Xin Wang*

MOE Key Laboratory of Pollution Processes and Environmental Criteria, Tianjin Key Laboratory of Environmental Remediation and Pollution Control, Research Center for Cleaner Production, College of Environmental Science and Engineering, Nankai University, No. 94 Weijin Road, Nankai District, Tianjin 300071, China

HIGHLIGHTS

- The power density was increased by 35% when the catalyst layer was unsintered.
- The hydrophobicity of the catalyst layer was increased after sintering.
- The enhancement was due to the increase of pores in the unsintered catalyst layer.
- Three phase interface of catalyst layer could exist in 6 μm pores.

GRAPHICAL ABSTRACT

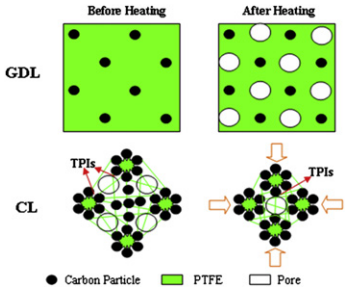

ARTICLE INFO

Article history:
Received 3 December 2012
Received in revised form
2 January 2013
Accepted 5 January 2013
Available online 16 January 2013

Keywords:
Air-cathode
Microbial fuel cells
Sintering
Activated carbon
Three-phase interface

ABSTRACT

The Pt and Nafion free air-cathode is urgently needed for large scale membrane-less single chambered microbial fuel cells (MFCs). The activated carbon air-cathode (ACAC) consisted of a sintered catalyst layer (CL) and a gas diffusion layer (GDL) made by rolling method is such a promising cathode with a high performance. However, the microstructure of the CL in terms of three phase interface (TPI) needs to be further investigated. The maximum power density increases by 35% from 802 ± 20 mW m^{-2} (3.40 ± 0.03 A m^{-2}) to 1086 ± 8 mW m^{-2} (2.80 ± 0.04 A m^{-2}) when the CL is not sintered. The maximum Coulombic efficiency (CE) also increases from 34% to 40%, possibly due to the decrease of hydrophobicity and the total volume/area of the CL. The total pore area and the porosity of the CL decrease by 87% and 42% after sintering, indicating that sintering reduced those pores among activated carbon aggregates so that TPIs are reduced. However, the available gas channel is produced when the GDL abundant of polytetrafluoroethylene (PTFE) is sintered.

1. Introduction

The single chambered air-cathode system is a promising configuration of microbial fuel cells (MFCs) to be scaled up for wastewater treatment due to its high power output, simple structure, and relatively low cost [1–3]. The performance of the air-cathode is mainly affected by the catalyst, the binder and the structure. Although the traditional catalyst of Pt and the binder of Nafion provide desired MFC performance, the high cost hampered its application in industrial scale [4]. Thus, one of the most advisable ways to reduce the cost is to optimize the structure of air-cathode without power decay. The effective conduction of proton/electron and access of reactant gas depend on the cathode

* Corresponding author. Tel./fax: +86 22 87030650.
** Corresponding author. Tel./fax: +86 22 23502756.
E-mail addresses: hongbingyu1130@sina.com (H. Yu), xinwang1@nankai.edu.cn (X. Wang).

0378-7753/$ – see front matter © 2013 Elsevier B.V. All rights reserved.
http://dx.doi.org/10.1016/j.jpowsour.2013.01.036

structure. The design of the gas diffusion layer (GDL) is essential for the gas transfer and water management, while the catalyst layer (CL) is crucial to oxygen reduction reaction (ORR) kinetics and three-phase interfaces (TPIs) [5]. Especially, a well designed CL improves the uniform gas diffusion and favors the reaction process [6].

In our previous work, a novel structure of scalable air-cathode without Nafion and Pt was developed by rolling activated carbon (AC) and polytetrafluoroethylene (PTFE) as porous CL (activated carbon air-cathode, ACAC) [7]. Such rolling ACAC has significant advantages of low cost, high reproducibility, scalability as well as comparable high performance (802 mW m^{-2}) over the air-cathode made by brushing PTFE as GDLs and a mixture of noble metal (e.g. Pt) and expensive binder (e.g. Nafion) as the CL (766 mW m^{-2}) [8]. Since the air-cathode needs to simultaneously provide three highways for oxygen, proton and electron to participate ORR at TPIs, a completely hydrophilic CL is adverse to the oxygen transfer in the CL through GDL leading to 'flooding' [9]. Reversely, if the CL is fully hydrophobic, the resistance caused by proton diffusion to CL will be a dominate factor to limit the power, which is called 'dry' [10]. In our rolling ACAC, appropriate amount of hydrophobic PTFE was used as the binder of AC to improve the porosity and enhance the gas transfer to TPIs. The PTFE is commonly needed to be melted in order to provide a thin film over the entire surface of the carbon black in the GDL and then to form gas pores after cooling down. This process is usually called sintering and takes place at temperatures around 320 °C [11]. For the air-cathode MFC made by the brushing method, sintering was also adopted after each PTFE layer was brushed on the carbon cloth [8]. However, for holding channels of proton besides that of gas, the PTFE content in the CL is much lower than that of the GDL. Thus, sintering of PTFE in the CL could result in an 'over hydrophobicity' and impede the proton transfer. Up to now, the effect of sintering on the PTFE binded CL of the air-cathode in MFCs had not been reported yet.

The main objective of this study is to assess the effect of the sintering treatment to the CL on the air-cathode performance in MFCs based on the microstructure change in the CL. The properties of the CL before and after sintering were investigated according to the contact angle measurement, mercury porosimetry method and scanning electron microscope (SEM), supplying reliable information of TPIs distribution formed by AC particles and the PTFE. On the basis of the parallel GDL, the ACACs with unsintered and sintered CLs were also evaluated in MFCs according to maximum power densities (MPDs), potentials of the anode and the cathode, Coulombic efficiencies (CEs) and cathodic biomass.

2. Experiments

2.1. The fabrication of air-cathode

The GDL film and the CL film were rolled as previously described [7]. 30 wt% carbon black (treated at 500 °C, Jinqiushi Chemical Co. Ltd, Tianjin, China) were distributed into an appropriate amount of pore-former ethanol in a beaker and ultrasonic agitated for 30 min at 30 °C, followed by dripping 70 wt% PTFE suspensions (60 wt%, Horizon, Shanghai, China, the mass ratio of carbon black to 60% PTFE was 3:7) into the blend slowly (Figure S1). It should be noted that all the PTFE content mentioned in the context was the content of PTFE suspension (60 wt%). After another 30 min, the blend was stirred and dried at 80 °C bath to give a dough-like paste. The paste was rolled to a GDL film of 0.35 mm in thickness. The GDL film was then rolled on one side of a square stainless steel mesh (16 cm^2, 0.3 mm in thickness) to make a flat sheet (0.4 mm in thickness). Six sheets were prepared and then sintered at 340 °C for 25 min for the subsequent CL rolling. The CL film was made in the same manner using ultracapacitor AC (treated at 800–1000 °C, 1500 m^2 g^{-1}, Xinsen Carbon Co. Ltd, Fujian, China) and PTFE with an optimal mass ratio of 6 (AC/60% PTFE). After the paste was rolled into a film of 0.35 mm in thickness, it was rolled on the opposite side of the GDL to form a final ACAC with a thickness of 0.6 mm. It should be noted that the thickness of electrode was not the sum of each film. Three ACACs were sintered at 340 °C for 25 min, while the other three were dried at 80 °C for evaporation of water and ethanol. The unsintered and sintered GDL films and CL films were simultaneously prepared for the mercury pore size analysis, contact angle measurement and morphological examination.

In order to investigate the influence of sintering on the CL, ratios of carbon material and PTFE used in our air-cathode here (6:1 for CL and 3:7 for GDL) were constant.

2.2. Contact angle measurements

Wetting measurements were performed using a JC2000D contact angle system (Powereach, Shanghai) under ambient conditions (25–30 °C, 30–35% relative humidity) using a horizontal light beam to illuminate the water droplet. Samples were supported on a horizontal stage and 7.0 μL drops of deionized water were deposited randomly across the surface for analysis. Contact angles were captured at moments of 0 min, 3 min, 6 min since the droplet contacted the sample surface and analyzed with the tangent method of Sessile Drop Fitting [11].

Young's equation was used to explain the balance of cohesive and adhesive forces of a liquid drop on a solid surface with a simple Equation (1) [12]:

$$\gamma^{sv} = \gamma^{sl} + \gamma^{lv}\cos\theta \quad (1)$$

where γ^{sv} represents the solid-vapor surface tension, γ^{sl} is the solid–liquid interfacial surface tension, γ^{lv} stands for the liquid–vapor surface tension and θ represents the contact angle ($0° < \theta < 180°$). The surface was defined hydrophobic in the case $\theta > 90°$, while the opposite ($\theta < 90°$) was hydrophilic. The hydrophobic degree increases as θ increases, and the hydrophilic degree increases as θ decreases.

2.3. Pore size distribution and surface morphology

The porous structure of the GDL and CL before and after sintering were characterized with a mercury porosimeter (Autopore IV, Micromeritics) which can analyze any porous media with a pore size ranging from 6 nm to 300 mm. Samples were firstly dried in an oven at 105 °C for 3 h in a stream of nitrogen, and then intruded volume analysis was carried out over the pressure ranging from 5 kPa to 414 MPa. After each change in pressure, the system equilibrates for 15 s to minimize overlap of the inter- (1–100 mm pore radius) and intra- (0.002–1 mm pore radius) porosity regions as determined by the porosimeter. Mercury porosimetric analysis allows quantification of the pore size and pore size distribution. The measurement principle is based on the law of capillary pressure governing liquid penetration into small pores. In the case of non-wetting liquid (contact angle, $\theta > 90°$), such as mercury, and assuming pores of cylindrical shape, this law can be expressed by the Washbum equation, shown in Equation (2) [13]:

$$D = -4\sigma_{Hg}\cos\theta_{Hg}/P \quad (2)$$

where D is the pore diameter (cm), P the applied pressure (Pa), σ_{Hg} the surface tension (dyn cm^{-1}), θ_{Hg} the contact angle (°). The values of σ_{Hg} and θ_{Hg} used in this study were 485 dyn cm^{-1} and 130°, respectively. During the measurement, larger pores were firstly

intruded with mercury. As the pressure increases, mercury gradually entered smaller pores. Different pressures correspond to different pore sizes. So the pore size distribution was obtained basing on the relationship between the pore size and the intruded mercury amount according to Equation (2).

The porous surface morphology of the GDL and CL before and after sintering was examined by SEM equipped with an energy-dispersive X-ray spectrometer (QUANTA 200, FEI Co., USA).

2.4. MFC tests

The single chambered MFCs were constructed as previously described [7]. Anodes were made of heated carbon mesh (450 °C for 30 min) [14], while cathodes were six ACACs. These anodes and cathodes were assembled tightly on opposite sides of six cylindrical Plexiglas chambers (4 cm long by 3 cm in diameter, net volume of 28 mL). Titanium wires were used to connect electrodes to the external circuit. Reactors were inoculated with effluent from an MFC operated for over half a year. The medium contained acetate (1.0 g L^{-1}), a phosphate buffer solution (50 mM PBS; NH_4Cl 0.31 g L^{-1}, KCl 0.13 g L^{-1}, $NaH_2PO_4 \cdot 2H_2O$ 3.321 g L^{-1}, Na_2HPO_4 4.090 g L^{-1}), and a trace mineral (12.5 mL L^{-1}) and vitamin (5 mL L^{-1}) solution [15], with a conductivity of 6.82 mS cm^{-1}. Reactors were operated in fed-batch mode at 30 °C and refilled with new medium solution when the voltage reduced below 30 mV, forming one cycle of operation (~2 days).

Cell voltages were measured every minute using a data acquisition system (PISO-813, ICP DAS Co., Ltd). Polarization curves were performed at the 3rd cycle after anodes were well acclimated. The maximum power densities (MPDs) were obtained from polarization curves by varying the external resistance from open circuit to 50 Ω. Each resistor was tested for 30 min. The power density ($P = IU/A$, I is the current (A), U is the voltage (V), A is the project area of the cathode (m^2)) and CE ($CE = C_{Ex}/C_{Th}$) were calculated as previously described [7]. Cathode and anode potentials were measured during polarization using an Ag/AgCl reference electrode (0.197 V versus standard hydrogen electrode).

Biomass on ACACs (60 d after inoculation) was evaluated on the basis of protein content measured according to the bicinchoninic acid method [16]. Six cathodes were taken out from MFCs and placed in a vial with 6 mL of 0.2 M NaOH, shaken to disperse the biofilm into solution. After that, they were rinsed with an additional 6 mL of deionized water. These liquids were combined, yielding a 12 mL sample that was then analyzed for protein content (all reagents from Baihao Biotechnology Co., Tianjin, China).

3. Results

3.1. The effect of sintering on wettability

The contact angle represents the wettability, which is determined by the cohesive forces of liquid molecules among themselves and adhesive forces resulting from molecular interactions between the liquid and solid, as presented in the supporting information (Figure S2) [17].

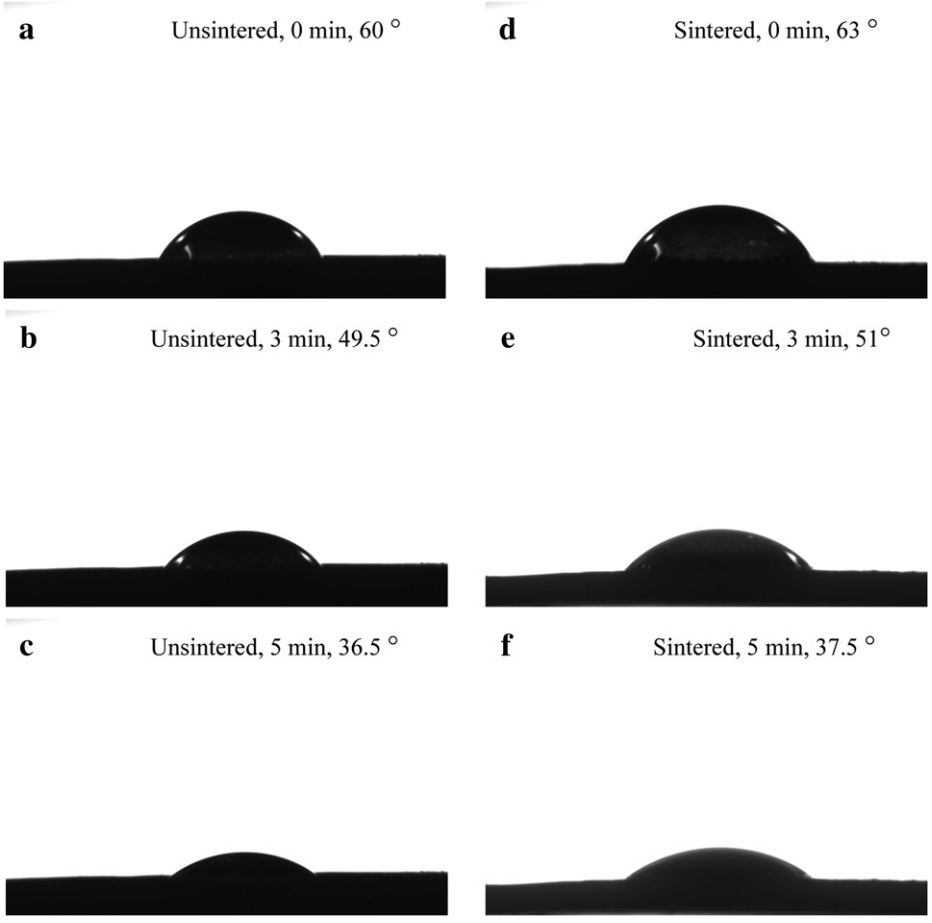

Fig. 1. Contact angles of water droplets on the unsintered CL film at (a) 0 min; (b) 3 min; (c) 6 min; Contact angles of water droplets on the sintered catalyst film at (d) 0 min; (e) 3 min; (f) 6 min.

In the GDL film with 70 wt% PTFE, contact angles were 103.5° (0 min), 101.5° (3 min) and 100° (6 min) in time sequence, with values all larger than 90° (Figure S3). It indicated that the sintered GDL film had a stable hydrophobicity so that the leakage of water can be avoided. Reversely, contact angles of unsintered CL film containing much less PTFE of 60° (0 min), 49.5° (3 min) and 36.5° (6 min) with values all smaller than 90° (Fig. 1). After sintering at 340 °C for 25 min, contact angles of CL film were slightly increased to 63° (0 min), 54° (3 min) and 37.5°(6 min). It can be also observed that in this case of AC/PTFE = 6 (mass ratio), the water droplet can be absorbed completely after several minutes for both samples, indicating that protons produced from the anode reaction in the electrolyte can easily migrate to TPIs to participate in ORR.

3.2. The effect of sintering on pore size and distribution

To investigate the effect of the sintering on the CL pore size, mercury intrusion porosimetry was carried out. The differential mercury intrusion of the unsintered GDL film with a PTFE content of 70 wt% was almost zero (Fig. 2a). It suggested that pores therein were too tiny (<6 nm) to be detected by the mercury porosimetric analysis. Only a small peak was observed near 6 nm during the exclusion of mercury (data not shown). For the same GDL film after the sintering treatment, with the pressure increased, the differential intrusion had a slight increase in the pore size (diameter) range from 30 to 60 μm. The amount of pores continuously increased as the size further decreased. For the pore size smaller than 30 μm, the differential intrusion exhibited a sharp increase and reached a maximum of 0.01 ml g^{-1} μm^{-1} at the pore size of 6 μm. Here the 6 μm stands for the densely pore distribution size. Comparing with those results of the unsintered GDL film, it was confirmed that these pores was formed owing to the PTFE rather than the carbon black which had been thermally treated before using. This was consistent with SEM images (Figure S4). Small conductive carbon aggregations were tightly binded with each other by PTFE during rolling, leaving no visible gas channel. In the process of sintering, PTFE was melted followed by contracting when cooled down and seems more smooth and intact (Figure S4). Due to the contraction of PTFE with carbon particles, the assorted size pores were formed. These hydrophobic pores were beneficial in oxygen transport and prevented the water leakage.

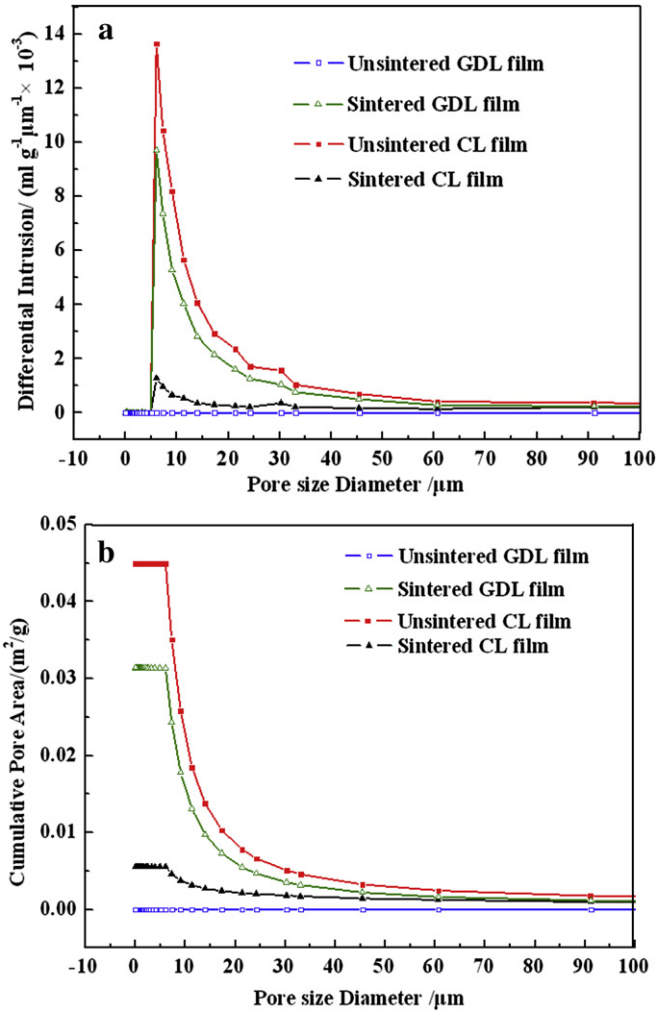

Fig. 2. The pore size distribution (a) and the cumulative pore area versus the pore size diameter (b) of the GDL film (PTFE of 70 wt%) and the CL film (PTFE of 14 wt%) before and after sintering.

However, an opposite result was obtained for the CL film with PTFE content of 14 wt%. It was clearly showed in Fig. 2a that the pore density of unsintered CL was higher than that of the sintered CL over all tested pore sizes. For the unsintered CL, with the increase of the pressure, the differential intrusion began to increase at the pore size of 60 μm, but the increase started much earlier from 20 μm for the sintered sample (Fig. 2a). Maximum differential intrusions of 0.014 ml g^{-1} μm^{-1} and 0.001 ml g^{-1} μm^{-1} were obtained at the same pore size of 6 μm for the unsintered and sintered CL film, indicating that the volume of pores in the CL film was reduced by 93% at this pore size after sintering. The cumulative pore area gradually increased with the pressure till no more mercury can be injected (Fig. 2b), and the total pore area, total intrusion volume and porosity were listed in Table 1. It can be figured out that the total pore area and the porosity of the CL film reduced by 87% and 42% respectively after sintering. The increase of median pore diameter after sintering was attributed to the sharp decrease in the density of 6 μm pore but not the actual increase of pore size. Accordingly in SEM images, it was showed that interlaced PTFE fibers connected AC aggregations on the surface of unsintered CL and formed many cavernous holes (Fig. 3a and b). However, both the space between AC aggregations and pore size were reduced after sintering (Fig. 3c and d). PTFE fibers were not as obvious as the unsintered CL.

3.3. Enhanced performance of MFCs by using unsintered CL

The open circuit voltage of the cathode with unsintered CL was 0.7 V (Fig. 4a). However, it reduced by 3% with the sintered CL. The MPD of MFCs equipped with unsintered CL (1086 ± 8 mW m^{-2} at 2.80 ± 0.04 A m^{-2}) was 35% higher than that of MFCs equipped with sintered CL (802 ± 20 mW m^{-2} at 3.40 ± 0.03 A m^{-2}).

Table 1
Results of the mercury porosimetric analysis for the GDL film and the CL film before and after sintering.

	GDL film		CL film	
	Unsintered	Sintered	Unsintered	Sintered
Total intrusion volume (mL g^{-1})	0	0.17	0.25	0.077
Total pore area (m^2 g^{-1})	0	0.031	0.045	0.006
Median pore diameter[a] (volume, μm)	0	39.09	41.79	140.08
Median pore diameter (area, μm)	0	9.92	9.95	135.50
Average pore diameter (4 V A^{-1}, μm)	0	21.97	22.37	55.99
Porosity (%)	0	7.39	9.75	5.62

[a] The median pore diameter stands for the pore size when the mercury intrusion percentage is 50%.

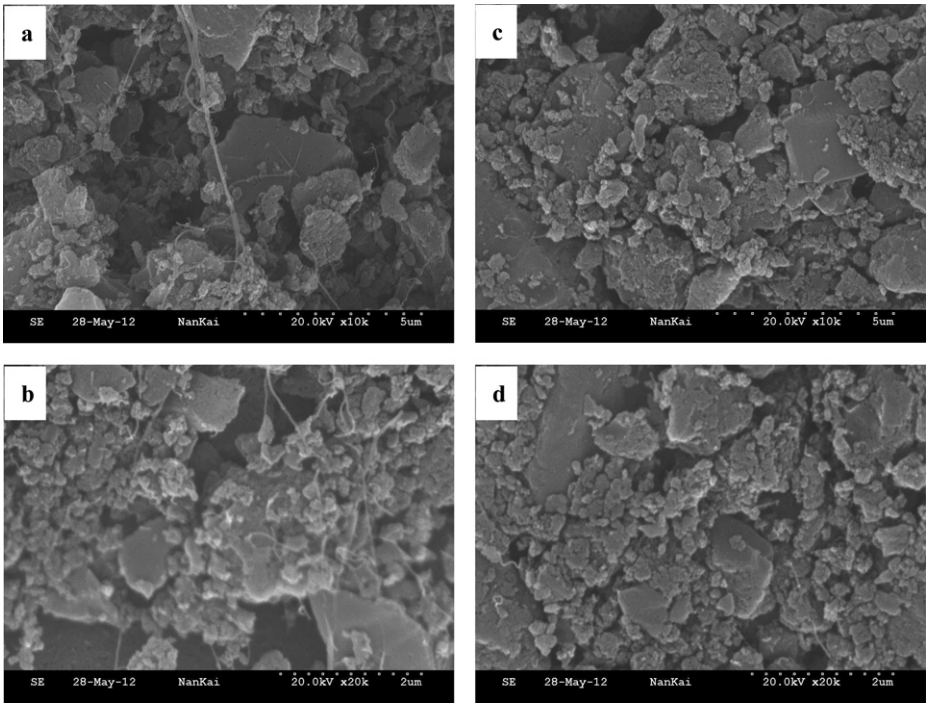

Fig. 3. SEM images of the unsintered (a, b) and the sintered CL (c, d) at the magnification of 10 k and 20 k.

It can be found in Fig. 4b that differences in the voltage between two MFCs with unsintered and sintered CLs were mainly due to cathode potentials. The open circuit potential (OCP) of the cathode with unsintered CL was 0.225 ± 0.002 V (vs. Ag/AgCl), which was 17% higher than 0.19 ± 0.04 V (vs. Ag/AgCl) obtained by the cathode with sintered CL.

CEs of MFCs with unsintered and sintered CLs increased with the increase of currents, which had the same trend as previous reports [18] (Fig. 4c). It was clearly showed that CEs were increased when the unsintered CL was used instead of the sintered CL on the ACAC. The maximum CE of the MFC with the cathode containing unsintered CL (40%) was 18% higher than that containing sintered CL (34%).

The biomass in terms of protein content on the cathode with unsintered CL was 320 ± 16 μg cm^{-2} (7 cm^2) after 30 cycles in MFCs. Under the same condition, the protein content was doubled (670 ± 13 μg cm^{-2}) on the cathode with sintered CL.

4. Discussion

There has been many deductive describes on the microstructure of the porous electrode in the field of fuel cell. For example, Watanabe et al. showed that there is a bimodal pore size distribution in the porous mass of carbon bonded with PTFE, with the boundary between the two pore classes at about 0.1 mm [19]. Kordesch et al. found that the primary (macro) structure of a porous electrode provided the skeleton of the electrode, and the secondary (micro) structure ensured gas transport [20]. However, no one is focused on the air-cathode in MFCs. During the thermal treatment above 320 °C, PTFE melts and crystallizes. Volatile precursors such as surfactants are removed [11]. According to contact angles and mercury intrusion porosimetry measurements, the sintering of GDL is essential for the PTFE to form hydrophobic pores for oxygen transfer (concentrated at 6 μm) and maintain a stable hydrophobicity to prevent water leakage. Reversely, as shown in Fig. 1 and Table 1, the sintering decreased the total pore volume/areas by 69%/87% and the porosity by 42% in the CL as well as weakened hydrophilicity of the CL surface. Especially, the range of pore size was decreased from <60 μm to <20 μm (Fig. 2), leading to a decrease in TPIs. This was confirmed by the decrease in power densities (35%) and cathode potentials (≥17%) (Fig. 4).

Excess oxygen (may be dissolved in water) diffused from the GDL through the CL to the electrolyte and caused the aerobic growth of cathodic biofilm, resulting in the major loss of charge. As described in Fig. 4c and cathodic biomass measurements, lower CEs of the sintered CL could be attributed to the sharp decrease in TPIs so that additional unadsorbed oxygen were consumed on the interface of the electrolyte and the CL by aerobic bacteria.

The reverse effect of sintering on the pore size of the GDL and the CL can be explained in view of their microstructures as illustrated in Fig. 5. In the unsintered GDL containing abundant PTFE, conductive carbon particles immersed in the PTFE without any gas space left, while the unsintered CL was composed of porous agglomerates of AC particles binded by the PTFE inside. Agglomerates were assumed spherically shaped and PTFE fiber network (Fig. 3a) was formed during the rolling process [7]. Small porous agglomerates were partially connected with each other to form bigger agglomerates, and partially were connected by the PTFE fiber network to be a compact body. Macropores around hydrophobic PTFE fibers were gas channels. It has been reported that the effective ORR takes place in those pores of micron dimension [19]. Oxygen diffused through macropores toward AC agglomerates and met protons in the thin film of electrolyte around hydrophilic AC. At the same time, electrons transferred to the solid AC from external circuit and reacted with oxygen and protons at these TPIs. After sintering at 340 °C for 25 min, the PTFE experienced a melting followed by contracting after cooling, leaving numerous gas transfer pores in the GDL. However, the contract of the PTFE net resulted in the reduction in the size of aggregates (the PTFE fiber integrated small aggregates), which was presented as the decrease of total pore volume. It should

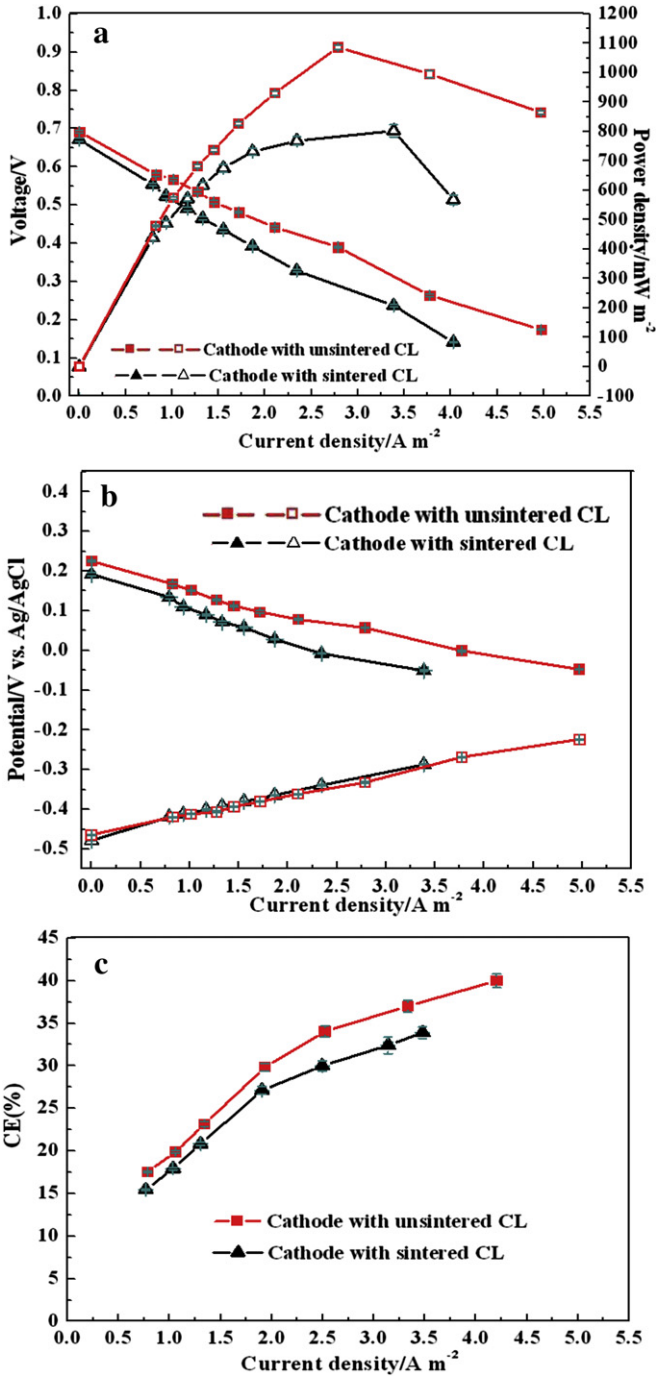

Fig. 4. Polarization and power density curves (a), electrode potentials (b) and Coulombic efficiencies of MFCs using unsintered and sintered CLs on the air-cathodes. Standard deviations were calculated based on the average result of three samples in each case.

be noted that the increase of average pore size was from the reduction of small pores among large aggregates (Fig. 2 and Table 1).

The optimization of TPIs in terms of pore volume and wettability is essential for the further increase in the performance of ACACs. As indicated by this study, pores with diameter size ranging from 6 μm to 60 μm were major oxygen channels for ORR and played important role in the 35% increase of MPDs. It should be noted that we cannot make a simple numeral comparison of the 1086 mW m^{-2} obtained here to ~3000 mW m^{-2} reported in previous literature

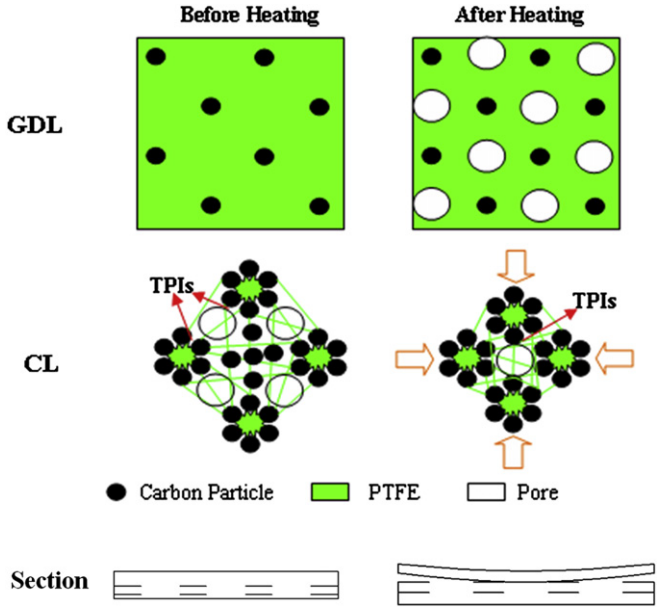

Fig. 5. The illustration of the overlook and side-looking microstructure of the CL and the GDL before and after sintering.

[21] because this value was obtained in an MFC with a 4 cm electrode spacing and the carbon mesh (a two dimensional material, not a three dimensional brush anode). It was believed that the power density can be extensively increased when the configuration and the anode material were optimized.

5. Conclusion

Maximum power densities of MFCs increased from 802 ± 20 mW m^{-2} to 1086 ± 8 mW m^{-2} by avoiding sintering of the CL. Contact angles of unsintered CL film slightly increased after sintering, suggested that the capacity of proton migration to TPIs in the CL was impaired. The total pore area and the porosity decreased by 87% and 42% after sintering in CL, indicating a decrease in gas channels and effective TPI areas during sintering. The densely pore distribution analysis showed that TPIs could be exist in 6 μm macropores. The biomass was doubled on the sintered CL compared to the unsintered CL after 30 cycles accompanied with a decrease of CE, which was caused by the bacterial consumption of excess oxygen diffused to the interface of the electrolyte and the CL. These results not only gave a detailed explanation of the power increase by avoidance of sintering in CL, but provided a new sight on how to further increase the performance of this activated carbon air-cathode in the future.

Acknowledgments

This research work was supported by the National Science and Technology Support Project (No. 2008BAC43B01), National Natural Science Foundation of China (Nos. 21107053 and 21037002).

Glossary

MFCs	microbial fuel cells
GDL	gas diffusion layer
CL	catalyst layer
ORR	oxygen reduction reaction
TPI	three-phase interface

AC	activated carbon
PTFE	polytetrafluoroethylene
ACAC	activated carbon air-cathode
MPDs	maximum power densities
CE	Coulombic efficiency

Appendix A. Supplementary data

Supplementary data related to this article can be found at http://dx.doi.org/10.1016/j.jpowsour.2013.01.036.

References

[1] D.H. Park, J.G. Zeikus, Biotechnology and Bioengineering 81 (2003) 348–355.
[2] H. Liu, B.E. Logan, Environmental Science & Technology 38 (2004) 4040–4046.
[3] H. Liu, R. Ramnarayanan, B.E. Logan, Environmental Science & Technology 38 (2004) 2281–2285.
[4] Z. Wen, S. Ci, F. Zhang, X. Feng, S. Cui, S. Mao, S. Luo, Z. He, J. Chen, Advanced Materials 24 (2012) 1399–1404.
[5] M. Prasanna, E.A. Cho, T.H. Lim, I.H. Oh, Electrochimica Acta 53 (2008) 5434–5441.
[6] H. Wang, Z. Wu, A. Plaseied, P. Jenkins, L. Simpson, C. Engtrakul, Z. Ren, Journal of Power Sources 196 (2011) 7465–7469.
[7] H. Dong, H. Yu, X. Wang, Q. Zhou, J. Feng, Water Research 46 (2012) 5777–5787.
[8] S. Cheng, H. Liu, B.E. Logan, Electrochemistry Communications 8 (2006) 489–494.
[9] U. Pasaogullari, C.Y. Wang, Journal of the Electrochemical Society 151 (2004) A399–A406.
[10] K.A. Klinedinst, W.M. Vogel, P. Stonehart, Journal of Material Science 11 (1976) 794–800.
[11] T.D. Astill, in: Chemistry, University of Victoria, 2003, p. 26.
[12] N.K. Adamm, Nature 180 (1957) 809.
[13] P. Gode, F. Jaouen, G. Lindbergh, A. Lundblad, G. Sundholm, Electrochimica Acta 48 (2003) 4175–4187.
[14] X. Wang, S.A. Cheng, Y.J. Feng, M.D. Merrill, T. Saito, B.E. Logan, Environmental Science & Technology 43 (2009) 6870–6874.
[15] D.R. Lovley, E.J.P. Phillips, Applied and Environmental Microbiology 54 (1988) 9.
[16] D.R. Bond, D.R. Lovley, Applied and Environmental Microbiology 69 (2003) 1548–1555.
[17] M. Ahn, Y.-H. Cho, Y.-H. Cho, J. Kim, N. Jung, Y.-E. Sung, Electrochimica Acta 56 (2011) 2450–2457.
[18] F. Zhang, T. Saito, S. Cheng, M.A. Hickner, B.E. Logan, Environmental Science & Technology 44 (2010) 1490–1495.
[19] M. Watanabe, M. Tomikawa, S. Motoo, Journal of Electroanalytical Chemistry 195 (1985) 81.
[20] K. Tomantschger, K.V. Kordesch, Journal of Power Sources 25 (1989) 195–204.
[21] C.s.I. Torres, H.-S. Lee, B.E. Rittmann, Environmental Science & Technology 42 (2008) 8773–8777.